

Electrotaxis of lung cancer cells in ordered three-dimensional scaffolds

Yung-Shin Sun,¹ Shih-Wei Peng,^{1,2} Keng-Hui Lin,^{1,3} and Ji-Yen Cheng^{1,2,4,a)}

¹Research Center for Applied Sciences, Academia Sinica, Taipei City 11529, Taiwan

²Institute of Biophotonics, National Yang-Ming University, Taipei City 11221, Taiwan

³Institute of Physics, Academia Sinica, Taipei City 11529, Taiwan

⁴Department of Mechanical and Mechatronic Engineering, National Taiwan Ocean University, Keelung 20224, Taiwan

(Received 23 September 2011; accepted 30 November 2011; published online 4 January 2012)

In this paper, we report a new method to incorporate 3D scaffold with electrotaxis measurement in the microfluidic device. The electrotactic response of lung cancer cells in the 3D foam scaffolds which resemble the *in vivo* pulmonary alveoli may give more insight on cellular behaviors *in vivo*. The 3D scaffold consists of ordered arrays of uniform spherical pores in gelatin. We found that cell morphology in the 3D scaffold was different from that in 2D substrate. Next, we applied a direct current electric field (EF) of 338 mV/mm through the scaffold for the study of cells' migration within. We measured the migration directedness and speed of different lung cancer cell lines, CL1-0, CL1-5, and A549, and compared with those examined in 2D gelatin-coated and bare substrates. The migration direction is the same for all conditions but there are clear differences in cell morphology, directedness, and migration speed under EF. Our results demonstrate cell migration under EF is different in 2D and 3D environments and possibly due to different cell morphology and/or substrate stiffness. © 2012 American Institute of Physics.

[doi:10.1063/1.3671399]

I. INTRODUCTION

Electrotaxis, or galvanotaxis, is the directional migration of adherent motile cells in response to an applied direct current (dc) electric field (EF). Over 150 years ago, endogenous dcEFs has been measured at epithelial wounds of human skins,¹ where DuBois-Reymond observed about 1 μ A of current leaving small epidermal wounds created in human fingers. It has long been proposed that, by sensing and orienting themselves toward such induced EF, cells are able to direct their movement toward the wounds to repair the damage.^{2,3} Such migration is also suggested to be related to the directional growth of cells and tissues during development and regeneration.⁴⁻⁶ To illustrate the underlying mechanism, many *in vitro* experiments have been performed to study the electrotaxis of various cell types in response to dcEFs with a magnitude of a few tens to hundreds of mV/mm, similar to that experienced *in vivo* (e.g., at human skin wounds). Many cells include lymphocytes,^{7,8} cancer cells,^{9,10} leukemia cells,³ and stem cells¹¹ were demonstrated to show evident electrotaxis effect. Some cells move toward the anode,¹²⁻¹⁴ and others migrate toward the cathode.^{8,15-17} Especially, a physiological dcEF originating from differential distribution of ion channels on polarized cells forms the so-called transepithelial potentials (TEP) which is reported to relate to the metastasis of cancerous tissues.^{18,19} However, the underlying mechanism of such correlation still requires further investigation to be clear.

In most electrotaxis experiments, cells are cultured and maintained on a two-dimensional (2D) flat substrate such as simple assembly of petri dishes and cover glasses^{3,20} or sophisticated glass- and/or polymethylmethacrylate (PMMA)- and/or polydimethylsiloxane (PDMS)-based

^{a)} Author to whom correspondence should be addressed. Electronic mail: jy Cheng@gate.sinica.edu.tw.

microfluidic chips,^{7–9} with dcEFs been applied via agar salt bridges^{3,9,20} or platinum electrodes.^{7,8} Though 2D electrotaxis experiment is easy and convenient to carry out in the aspects of manipulation and observation, it may fail to capture some *in vivo* conditions where cells are situated in 3D microenvironment. The effect of the electric field may be different in cell movement over three-dimensional (3D) topology compared with 2D flat substrates.

Tissue cells in the human body grow in a 3D microenvironment composed of extracellular matrix, carbohydrates, and other cells. A number of studies have been done to reveal the effects of 2D versus 3D cell culture on differentiation,^{21–25} drug metabolism,^{26–30} gene expression and protein synthesis,^{31–35} general cell function,^{36–40} increase of *in vivo* relevance,^{31,41–43} morphology,^{44–47} proliferation,^{26,48–51} response to stimuli,^{41,52–54} viability,^{36,55–57} and migration.^{58–61} Adding the third dimension to cellular environment provides them with more *in vivo*-like morphology, behaviors, and intercellular interactions for understanding cytology in more physiological conditions.

3D scaffolds are introduced to mimic cells' *in vivo* environment while cultured *in vitro*. The scaffolds often are highly porous for seeding cells inside and providing large surface areas for cell migrations and interactions. Conventional methods for fabricating 3D porous scaffolds include phase separation,^{62,63} electrospaying,⁶⁴ electrospinning,^{65,66} particle leaching,⁶⁷ and others.⁶⁸ Scaffolds made by these methods often exhibit inhomogeneous structures with uncontrollable and unpredictable pore sizes and reduced inter-pore connections. It is hard to do systematic analysis on the cell-matrix interactions on such platforms. Recently, various methods have been developed for producing 3D ordered scaffolds via solid freeform fabrication techniques such as fused deposition modeling,⁶⁹ shape deposition manufacturing,⁷⁰ stereolithography,⁷¹ selective laser sintering,⁷² and 3D printing.⁷³ A majority of these methods involve complicated processes and/or expensive robots, so they are not suitable for massive scaffold fabrication. Recently, Lin *et al.*⁷⁴ reported using simple microfluidics to easily and economically fabricate 3D scaffolds with uniform pore sizes by generating monodisperse foam with a microfluidic device.

In this study, a modified microfluidics based on the above mentioned system was used to fabricate 3D ordered porous scaffolds.⁷⁵ The pores of the scaffold are spherical and uniform in diameter ranging from 80 to 100 μm and provide alveoli-like structure. Using microfluidics provides an easy and economical way to fabricate 3D scaffolds with uniform pore sizes. The base material of the scaffold is crosslinked gelatin which is good for cell adhesion and proliferation. After seeding cells, scaffolds were embedded in a tightly sealed fluidic chamber. The cell morphology was compared with that on 2D substrate. The fluidic chamber was then integrated with two agar salt bridges for EF application and a transparent heater for temperature control. Compared to traditional electrotactic systems which often have problems in medium evaporation and temperature maintenance,⁷⁶ the presently designed chamber provides better control over the experimental microenvironment. The size of the chamber and thus the medium consumption are largely reduced. The electrotaxis effect of human lung cell lines, A549, CL1-0, and CL1-5,^{77–79} in 3D scaffolds was observed and compared with that studied in 2D gelatin-coated and bare substrates.⁹

II. MATERIALS AND METHODS

A. 3D scaffold fabrication

A PDMS-based flow-focusing device was used to generate monodisperse foam (Fig. 1(a)). At a temperature-controlled environment, a solution of 7% gelatin (Sigma) and 1% Pluronic[®] F127 surfactant (w/w % in warm de-ionized (DI) water) was injected into the liquid inlet while nitrogen gas passed through the gas inlet. Under the appropriate air pressure and liquid flow rate controlled by pressure regulator and syringe pump, respectively, monodisperse bubbles at crystalline packing fraction were produced (Fig. 1(b)) and collected at the outlet into customized reservoirs. Afterwards liquid gelatin foam were first congealed in 4 °C refrigerator for 5 min, transferred into a solution of 2% formaldehyde (Sigma) and 0.1% glutaraldehyde (Sigma) (w/w % in DI water) at 4 °C overnight for chemical crosslinking. The resulting solid

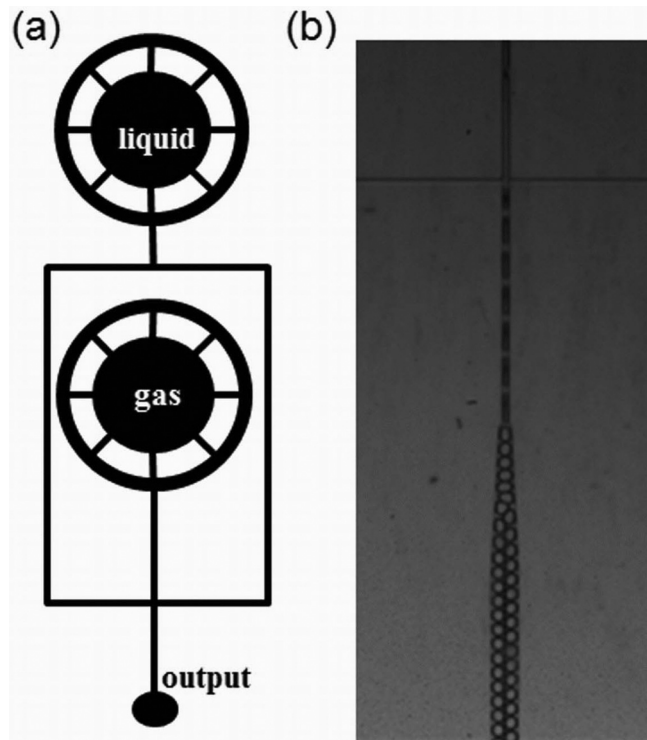


FIG. 1. (a) PDMS-based micro-channel device with solution and gas has been pumped through the inlets and bubbles have been collected from the outlet. (b) Monodisperse bubbles with a uniform size were formed and constantly flowed out.

foam was further degassed under vacuum to become scaffold with interconnected pore structure. To be biocompatible, the scaffolds were washed extensively in DI water for 1 h and then in 1 M glycine (Sigma) for another hour, washed in the same order for two more times, and stored in phosphate buffered saline (PBS) under 4 °C before further use.

B. Fluidic chamber fabrication

As shown in Fig. 2, the fluidic chamber consists of 3 pieces of PMMA substrates, 3 pieces of double sided tapes (8018, 3M), and 1 piece of glass slide. The pattern was designed in AutoCAD (Autodesk) and then loaded in a CO₂ laser scriber (M-300, Universal Laser Systems or ILS2, Laser Tools & Technics Corp.) to ablate desired pattern on PMMA substrates (thickness = 1 mm) and double sided tapes (thickness = 70 μm). Two protrudent pieces (3 mm × 4.5 mm each) of the middle PMMA were used to clip the scaffold and prevent it from sliding away during observation. The empty channel of the bottom PMMA is 50 mm × 12 mm in dimension. The top PMMA have 4 holes on it, with the middle two (diameter = 5 mm each) glued to bigger adapters for agar salt bridges and the outside two (diameter = 2 mm each) glued to smaller adapters for medium flow. In our early studies,⁹ cytotoxicity of the double sided tapes on CL1-5 cells was examined, and no significant change in cell viability was observed.

C. EF calculation and measurement

According to Ohm's law, the strength of electric field through a bulk material is

$$E = I/\sigma A_{eff}, \quad (1)$$

where I is the electric current flowing across the material, σ is the conductivity of the material, and A_{eff} is the effective cross-sectional area of the material. Equation (1) is used to calculate the EF inside the fluidic chamber where no scaffold is presented. The actual EF inside the

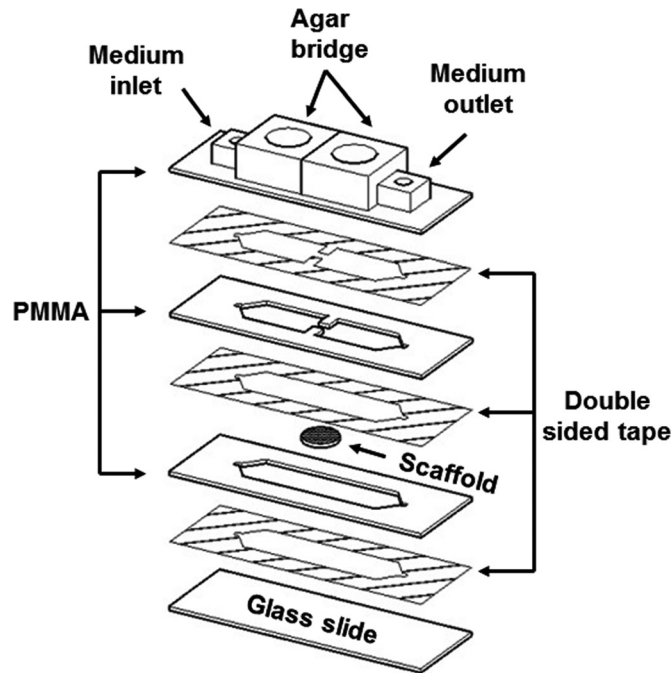


FIG. 2. Design of the fluidic chamber assembly.

scaffold-containing chamber was measured as the following. On the top PMMA (see Fig. 2), few more holes (diameter = 1.08 mm) were fabricated by laser ablation in the middle area between two agar salt bridges. Shielded copper wires were inserted into the scaffold through these holes and tightly glued. Potential difference between any two of these holes was measured using an oscilloscope (TDS2024, Tektronix). The EF was calculated to be the potential difference divided by the distance between the holes.

D. Cell preparation

Lung cancer cell lines CL1-0 and CL1-5 were kindly provided by Pan-Chyr Yang (from National Taiwan University, College of Medicine).^{77,79} Lung cancer cell line A549 was purchased from Bioresource Collection and Research Center (BCRC), Taiwan. A complete medium composed of Dulbecco's Modified Eagle's medium (DMEM, Gibco) and 10% fetal bovine serum (FBS, Invitrogen) was used for all cells. Cells were incubated in tissue culture poly-styrene (TCPS) flasks (Corning) in 5% CO₂ at 37 °C before seeding into the scaffolds.

E. Electrotaxis experiment

20 μ l cell suspension at a density of $5 \times 10^6 \sim 10^7$ cell/ml was pipetted into the scaffold, and then the scaffold was incubated in 5% CO₂ at 37 °C for at least 2 h. During this time, cells were able to penetrate into deeper layers of the scaffold through interconnected pores, and further adhere onto the walls of the pores. PMMA substrates were then assembled by double sided tapes in an upside-down way, and the scaffold was placed in the middle of two protrudent pieces with cell-seeded side facing up (Fig. 2). The glass slide was last glued beneath the PMMA layers to form the fluidic chamber. The device was further connected to two agar salt bridges (1.5% agar dissolved in PBS) via the middle two adapters, and to two plastic tubes via the outside two adapters. DMEM only (without serum) was pumped into the chamber manually until the volume was filled.

For electrotaxis study, the fluidic chamber was mounted on top of a transparent indium tin oxide (ITO) glass (Part No. 300739, Merck) which was connected to a proportional-integral-derivative (PID) controller (TTM-J4-R-AB, JETEC Electronics Co.) for maintaining temperature

at $37 \pm 0.5^\circ\text{C}$ via feedback from a thermal couple (TPK-02 A, TECPEL) clamped tightly between the heater and the chamber. For bright-field imaging, the chamber-heater unit was clipped onto the xy stage of an inverted microscope (IX71, Olympus) for cell observation using a 20X objective lens. For 3D bright-field/fluorescent imaging, the unit was mounted onto the xyz stage of a spinning disc confocal microscope (CSU22, Hamamatsu) using a 20X water immersion objective lens. The whole system for electrotaxis experiment is illustrated in Fig. 3. To apply EF through the chamber, agar salt bridges were placed in beakers filled with PBS, where Ag(anode)/AgCl(cathode) electrodes were connected to a dc power supply (PowerPac Basic, Bio-Rad) in series with a multimeter (189, Fluke) for continuously monitoring the current. Usually, a voltage of 80 V was applied on the electrodes, which gave a measured current of around 6 mA.

F. Cell migration measurement

We observed cell migrating inside pores of the second or third layer of the scaffolds from the bottom surface by the bright-field inverted microscope. Time-lapse movie was taken at an interval of 5 min for 2 h with a digital camera (Canon 500D) and analyzed by ImageJ software (National Institute of Health (NIH)). We quantified the migration directedness and speed by tracing the position of the cells. The migration directedness is defined as the average cosine θ , $(\sum_i \cos\theta_i)/n$, where θ is the angle between the vector of applied EF (from positive to negative) and the vector from the start to the end position of a cell, and n is the total number of cells taken into consideration. A directedness of -1 means that all cells move toward the cathode, while $+1$ indicates all cells migrating toward the anode. The directedness of a group of randomly walking cells should be close to 0. The migration speed is defined as the average displacement (in xy plane) of cell migration per hour. For each type of cells with or without the applied EF, more than 50 cells were selected from 2 to 6 independent experiments for data analysis. Standard error of the mean (SEM) was added to the data. Statistical differences between experimental and control groups were assessed with unpaired Student's t -test with p -values shown in corresponding figures.

G. Electrotaxis experiment of lung cancer cells on 2D gelatin substrates

A microfluidic cell culture chip reported in our early work⁹ was slightly modified and used for studying cells' migration on 2D gelatin-coated substrates. First, regular cover glasses (60 mm \times 24 mm) were immersed into a solution of 5% aminosilane (3-aminopropyl-triethoxysilane, Fluka) in DI water (w/w %) for 2 min, removed slowly out of the solution, and baked at

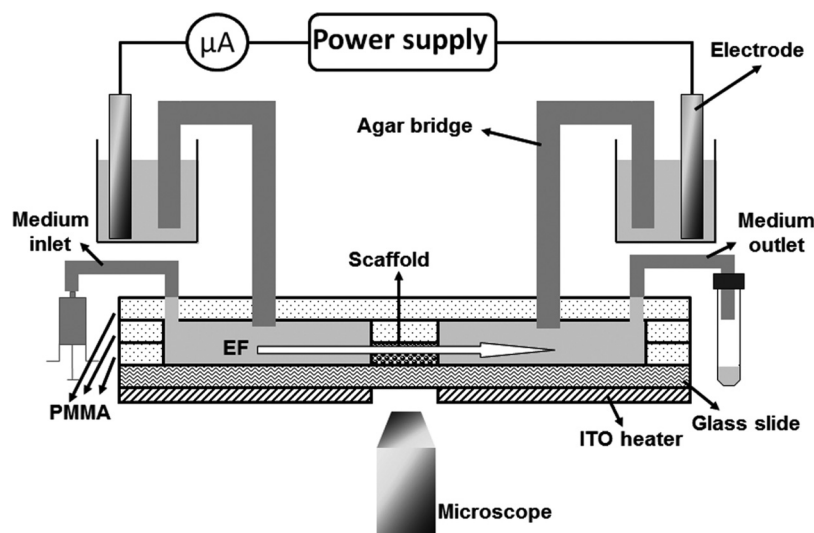


FIG. 3. Side-view of the electrotaxis system.

80 °C for 20 min. A double sided tape with a trench size of 27 mm \times 5 mm was stuck onto an aminosilane-treated glass. 10 μ l of gelatin solution (see Sec. II A) was pipetted onto the trench area and then spin-coated evenly over that area. The volume of gelatin solution was calculated to ensure that it covered the whole trench surface with a height equal to that of the tape (70 μ m). For crosslinking, the gelatin-coated glass was immersed in 2% formaldehyde (w/w % in DI water) for 1 h and washed in DI water and glycine as described in Sec. II A. Assembly of the microfluidic chip was detailed in our early work.⁹ For electrotaxis experiments, cells in identical conditions (i.e., density and medium, see Sec. II E) were infused manually into the chamber and cultured overnight. Serum-free medium was used when the EF was applied and electrotaxis experiment was carried out. Cell observation and migration measurement are described in Secs. II E and II F.

III. RESULTS

A. 3D scaffolds with a uniform pore size

As shown in Fig. 1(b), uniform-sized bubbles packed in the crystalline state⁷⁴ were collected from the outlet into a PMMA-made reservoir. After degassed under vacuum, the interconnected pores were filled with water. The size of the reservoir as well as the scaffold is 1 mm in thickness and 6 mm in diameter as shown in Fig. 4(a). Fig. 4(b) shows a bright field image of the scaffold. Pores in each plane are often arranged in honeycomb order and a different layer of pores can be seen from the blur out-of-focus image. Fig. 4(c) shows a better sectioning image of fluorescence imaged by a confocal microscope. The edges around the pores

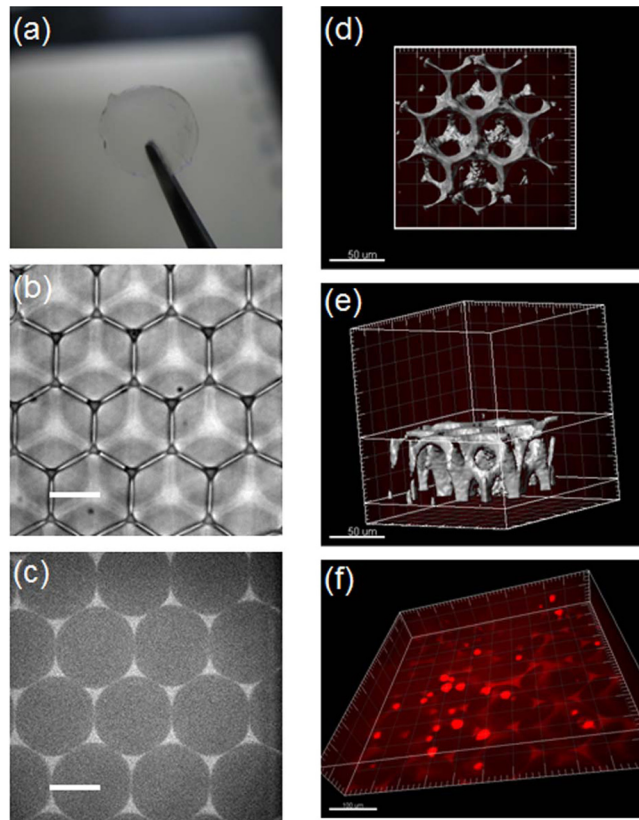


FIG. 4. (a) Picture of a 3D scaffold. (b) Bright-field confocal image of a 3D scaffold. Only one fixed layer is shown. Scale bar = 50 μ m. (c) Fluorescent confocal image of a 3D scaffold. Only one fixed layer is shown. Scale bar = 50 μ m. (d) Re-constructed 3D top-view image of a 3D scaffold. (e) Re-constructed 3D side-view image of a 3D scaffold. (f) Re-constructed 3D image of CL1-0 cells (stained with CellVue[®]) inside a 3D scaffold (enhanced online) [URL: <http://dx.doi.org/10.1063/1.3671399.1>].

are not uniform in thickness. 3D structures of the scaffold were re-constructed from a z -dimensional stack of Fig. 4(c) using Imaris 7.0.0 (Bitplane). Fig. 4(d) shows the top-view of the scaffold, where the size of top-to-bottom connected pores is around $50\ \mu\text{m}$. Furthermore, Fig. 4(e) shows the side-view of the scaffold, where the size of side-to-side connected pores is about $20\text{--}30\ \mu\text{m}$. These pore sizes are large enough for cells to penetrate down to deeper layers as well as to migrate horizontally from one pore to another. CL1-0 cells stained with CellVue[®] (peak excitation at 655 nm and peak emission at 675 nm) were pipetted onto the surface of a scaffold and then incubated for 2 h as mentioned in Sec. II E. This cell-seeded scaffold is shown in Fig. 4(f), which was re-constructed from a stack of confocal images in the z dimension. It is clear that cells with a size of $10\text{--}20\ \mu\text{m}$ stayed in different layers and positions of the scaffold. See Movie 1 for the 3D structure of Fig. 4(f).

Although having different surface chemistry, such 3D porous scaffolds share many similar characteristics with the *in vivo* pulmonary alveoli (see Fig. 5). First, an alveolus has a form of a hollow cavity, with an average diameter of $200\text{--}300\ \mu\text{m}$. Second, in some alveolar walls, there are pores between alveoli called Pores of Kohn. Last but not the least, the stiffness of these gelatin-made scaffolds was measured to be $3\text{--}10\ \text{kPa}$ by tissue deformation stage (Harrick Scientific).⁸⁰ Such stiffness is similar to that of the alveoli ($1.5\text{--}2\ \text{kPa}$ (Ref. 81)), but many orders of magnitude smaller compared with that of glass ($50\text{--}90\ \text{GPa}$) or PMMA ($1.8\text{--}3.1\ \text{GPa}$). Table I summarizes the similarities between 3D porous scaffolds and pulmonary alveoli. All these features rationalize our choice of such scaffolds for *in vitro* studying lung cancer cell behaviors.

B. Comparison of cell morphology in 2D and 3D environments

We observed that CL1-5 and A549 cells cultured inside 3D scaffolds have very different morphology compared to those cultured on flat 2D substrates. Figure 6 shows the ellipticity, defined as $[(\text{long axis}) - (\text{short axis})] / (\text{long axis})$ for an ellipse-shaped cell, of (a) CL1-0, (b) CL1-5, and (c) A549 cells after 2 h and 2 days cultured in 2D and 3D environments. In 3D environments, the ellipticity is calculated by the projected 2-dimensional image, so the value will be slightly underestimated. A round-shaped cell has an ellipticity of 0. It is noticed that, for all the three cell lines, cell morphology does not differ significantly between 2D (2D glass surface) and 2DG (2D-gelatin coated) surfaces. However, when cultured in 3D (3D-gelatin made scaffold), CL1-5 and A549 showed significant morphology changes. CL1-0 cells have

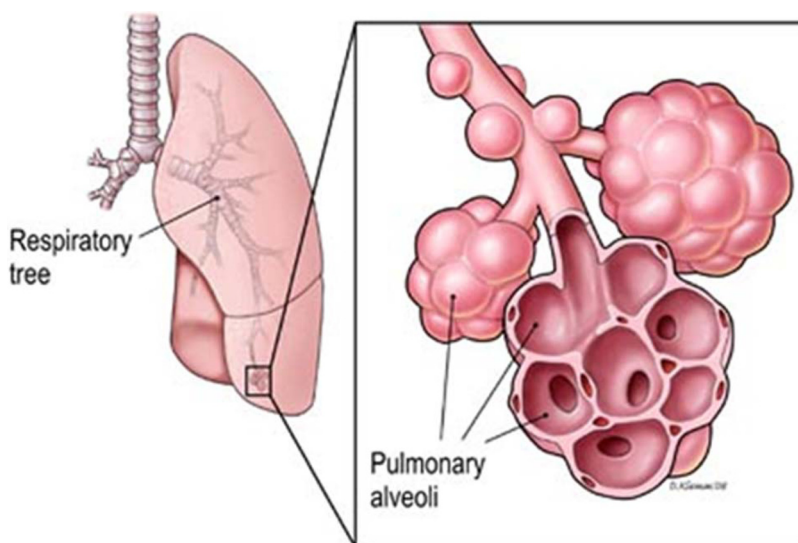


FIG. 5. Pulmonary alveoli. An alveolus has a form of a hollow cavity, and in some alveolar walls, there are pores between alveoli called Pores of Kohn (reprinted from The President's Council on Bioethics, Washington, D.C., January 2009, <http://bioethics.georgetown.edu/pcbe/>).

TABLE I. Similarities between 3D porous scaffolds and *in vivo* pulmonary alveoli.

Characteristics	3D porous scaffolds	Pulmonary alveoli
Made of pores/bubbles	YES, diameter = 80 μm	YES, diameter = 200–300 μm
Interconnected pores	YES, top-bottom: 50 μm ; side-side: 20–30 μm	YES, Pores of Kohn: 3–20 μm
Stiffness	3–10 kPa	1.5–2 kPa

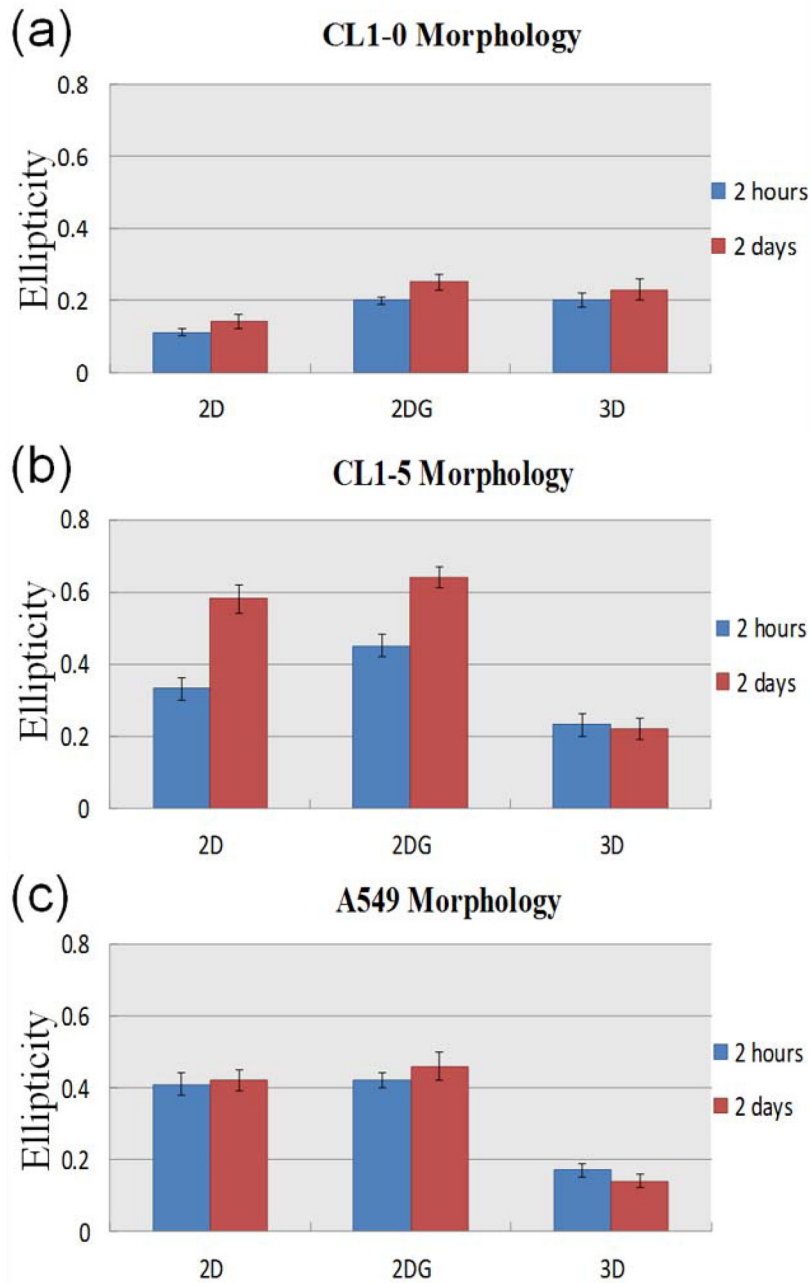


FIG. 6. Ellipticity of (a) CL1-0, (b) CL1-5, and (c) A549 cells after 2 h and 2 days cultured in 2D and 3D environments. (2D: 2D bare substrate, 2DG: 2D-gelatin coated substrate, 3DG: 3D-gelatin made scaffold.) For each cell line, the total number of cells selected for analysis is 30.

similar ellipticity (0.1–0.2) when cultured 2-dimensionally and 3-dimensionally. But, take 2-day culturing for example, CL1-5 cells have an average ellipticity of 0.22 in 3D scaffolds, compared to 0.58–0.64 in 2D bare and gelatin-coated glass substrates, and A549 cells have an average ellipticity of 0.14 in 3D scaffolds, compared to 0.42–0.46 in 2D substrates. CL1-5 and A549 cells exhibit different morphology when cultured in 2D and 3D environments likely in response to the physical/mechanical properties of their surrounding materials, and this might in turn affect their responses to EF stimuli as described in Secs. III C–III E.

C. EF calculation and measurement

Referring to Eq. (1) of Sec. II C, in the present system, I is the applied direct current in mA, $\sigma = 1.38 \Omega^{-1} \text{ m}^{-1}$ for DMEM and $A_{\text{eff}} = 15 \text{ mm}^2$ for geometry shown in Fig. 2, which give a constant $E = 48.3 \times I \text{ mV/mm}$ throughout the chamber where no scaffold is presented. At an applied voltage of 80 V on the electrodes, a current of 6 mA was measured on the multimeter. This in turn gives a calculated EF strength of 290 mV/mm of no scaffold. However, the measured EF inside the scaffold was 338 mV/mm, which is about 16% higher than the calculated value. Simulation was performed (data not shown) and showed good agreement with the measurement. The increase in EF is mainly due to the porous structure of 3D scaffolds where the effective cross-sectional area is smaller in Eq. (1) compared to the situation without scaffolds.

D. Cell migration under dcEF inside 3D scaffolds

As described in Sec. II E, cell migration was observed and imaged by an inverted microscope using a 20X objective lens. This gives a field of view (FOV) of about $1 \text{ mm} \times 1 \text{ mm}$, which is large enough for the observation without the need of moving the stage. Cells moved out of focus or FOV were not selected for analysis. Lung cancer cell lines CL1-5 and A549 have been shown to migrate with clear directivity under dcEF in traditional 2D environments.^{9,10} In our present study, cells were seeded into 3D ordered scaffolds, and their movement under an applied EF of 338 mV/mm was observed. Figs. 7(a) and 7(b) (Movie 2) show images of lung cancer A549 cells under EF at $t = 0 \text{ min}$ and $t = 60 \text{ min}$, respectively (see Movie 2 for the cell migration in 3D scaffold). We observed the cells located in the second layer of the scaffold, and some of them were able to move across neighboring pores through interconnected pores (e.g., cells in circles). However, as seen in the video, some cells could not penetrate the circular pore, mainly because they were blocked in the boundary of the pore where no interconnected pores exist. This observation suggests that lung cancer cells can freely migrate inside and may, therefore, penetrate through *in vivo* pulmonary alveoli during their infection and/or metastasis. The foam scaffold may be used as a model system to study lung cancer cell migration.

The migratory behaviors of CL1-0, CL1-5, and A549 cells were shown as polar plots in Fig. 8. At $t = 0 \text{ min}$, cells were set at the origin, and their positions after 2 h with (right column) and without (left column) the applied EF were recorded in the plots. Without EF, all types of cells moved randomly and showed no directional tendency. Under an applied EF of 338 mV/mm, the directivity of different cells was clearly observed: CL1-0 cells showed no bias, CL1-5 cells migrated toward the anode, and A549 cells moved toward the cathode. These directional migrations in 3D environment imply that electrical potential (endogenous or extrinsic) is possibly one major factor affecting the metastasis and activity of lung cancer cells *in vivo*. The directedness of 3 different cell lines is listed in Table II. Under EF, CL1-0 cells did not show prominent directional movement (directedness = 0.06 ± 0.05 compared to 0.11 ± 0.09 without EF), while CL1-5 cells migrated toward the anode (directedness = -0.33 ± 0.10 compared to 0.02 ± 0.11 without EF, $p < 0.01$), and A549 cells migrated toward the cathode (directedness = 0.25 ± 0.04 compared to -0.05 ± 0.09 without EF, $p < 0.05$). CL1-5, though derived from CL1-0, does exhibit obvious directedness and is more invasive than its parent cell line both *in vivo* and *in vitro*.^{78,79} Global genomic analysis has shown the gene expression difference between these two sublines.⁷⁸ Another interesting finding is that about 10%–20% of CL1-5 cells, which are ellipse-shaped (see

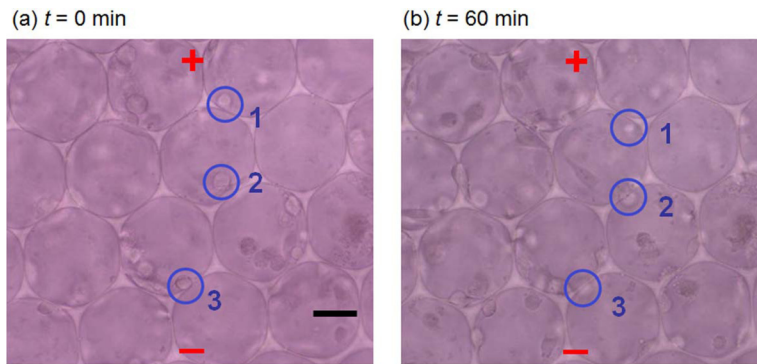


FIG. 7. A549 cells inside a 3D scaffold under an applied EF of 338 mV/mm at (a) $t=0$ min and (b) $t=60$ min. Clearly some cells (Nos. 1, 2, and 3 in blue circles) migrated through interconnected pores (enhanced online) [URL: <http://dx.doi.org/10.1063/1.3671399.2>].

Sec. III B), tend to orient themselves perpendicularly to the EF direction. This might cause some steric hindrance to cells when they tried to move across interconnected pores. A rough counting estimated that 5%–10% of round-shaped cells and only less than 1% of ellipse-shaped cells could migrate through interconnected pores, depending on their locations (in the middle or edge of

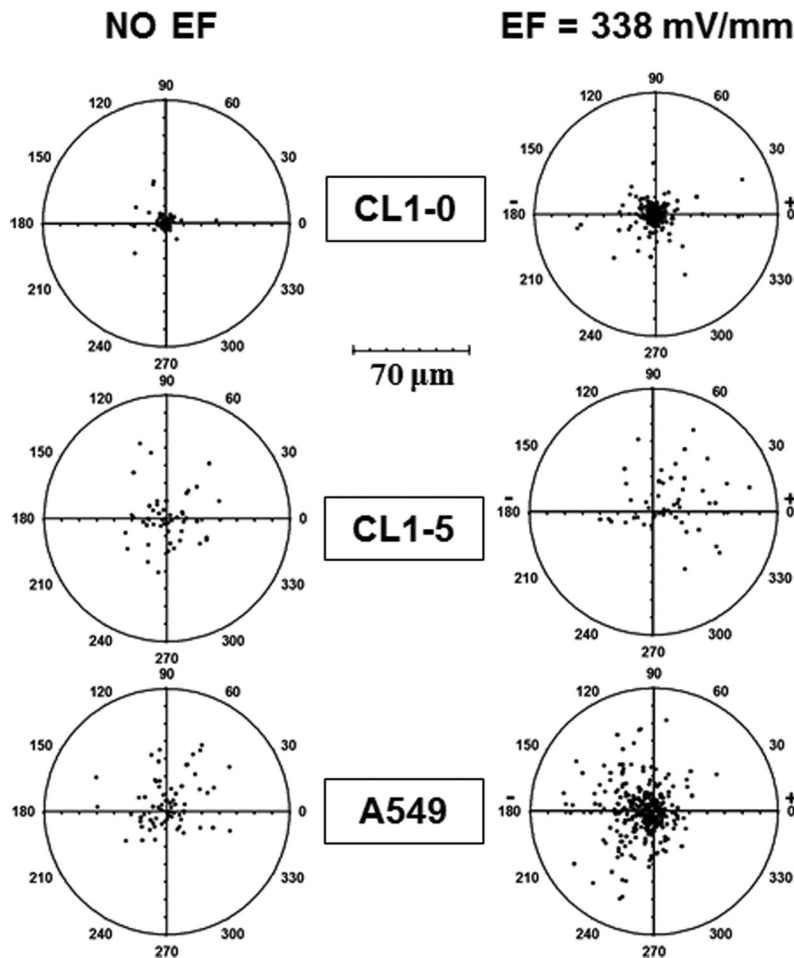


FIG. 8. Polar plots of cell migration after 2 h with and without the applied EF. Left column: CL1-0, CL1-5, and A549 without the applied EF. Right column: CL1-0, CL1-5, and A549 with the applied EF of 338 mV/mm. In the beginning, cells are set at the origin. All plots have the same scale and EF direction (from the right to the left).

TABLE II. Migration directedness and speed of 3 different cells with and without the applied EF in 3D scaffolds. n is the total number of cells selected for analysis.

With EF	Directedness \pm SEM	Speed \pm SEM ($\mu\text{m}/\text{h}$)
CL1-0 ($n = 232$)	0.06 ± 0.05	3.63 ± 0.27
CL1-5 ($n = 50$)	-0.33 ± 0.10	11.56 ± 1.11
A549 ($n = 308$)	0.25 ± 0.04	7.73 ± 0.36
Control group	Directedness \pm SEM	Speed \pm SEM ($\mu\text{m}/\text{h}$)
CL1-0 ($n = 83$)	0.11 ± 0.09	2.21 ± 0.45
CL1-5 ($n = 51$)	0.02 ± 0.11	8.01 ± 0.77
A549 ($n = 67$)	-0.05 ± 0.09	8.4 ± 0.71

pores) and migrating directions (toward interconnected pores or not). The shape effect manifests itself in the 3D scaffold where steric hindrance exists. On the contrary, the cell shape does not affect the migration in 2D substrate. Detailed comparison of electrotactic response between cells cultured in 2D and 3D environments is discussed in Sec. III E. We have also studied the differences in gene expression levels under EF stimulation in an ongoing project.⁸² Our preliminary results revealed that some genes were up-regulated while some were down-regulated, and these could imply the influence on cells' metastatic pathways.

Table II also shows the migration speed of CL1-0, CL1-5, and A549 cells. Both CL1-0 and CL1-5 exhibited higher motility than A549 in response to an applied EF. For example, CL1-5 cells under $\text{EF} = 338 \text{ mV}/\text{mm}$ moved about 1.5 times as fast as those without EF stimulation. The EF not only direct but also speed up cell migration.

E. Comparison of cell migration under dcEF in 2D and 3D environments

Table III lists the migration directedness and speed of lung cancer cell lines CL1-0, CL1-5, and A549 under $\text{dcEF} = 300\text{--}375 \text{ mV}/\text{mm}$ in 2D (bare substrates^{9,10} and gelatin-coated glasses) and 3D (gelatin-made scaffolds) cultures. First, cells in all environments showed identical migration directions, being CL1-0 had no bias (near-zero directedness), CL1-5 moved toward the anode (negative directedness), and A549 migrated toward the cathode (positive directedness). However, for CL1-5 and A549 cells, the absolute values of directedness are different in three environments, being 3D scaffolds $<$ 2D gelatin-coated glasses $<$ 2D bare substrates (for CL1-5, $0.33 < 0.43 < 0.60$; for A549, $0.25 < 0.31 < 0.76$). 3D cells showed the weakest electrotactic response (i.e., the smallest directedness) because not all of them were able to migrate freely inside such scaffolds. This steric hindrance causes some cells to be blocked by the walls of the pores. Also, as described in Sec. III A, 3D scaffolds composed of gelatin are softer (stiffness \sim kPa) than 2D gelatin-coated glasses (stiffness \sim 100 kPa) and bare glass or PMMA

TABLE III. Electrotaxis of lung cancer cell lines CL1-0, CL1-5, and A549 in 2D and 3D environments. Stimulation time = 2 h (2D: 2D bare substrate, 2DG: 2D-gelatin coated substrate, 3D: 3D-gelatin made scaffold).

Cell type (mV/mm)	Directedness \pm SEM	Speed \pm SEM ($\mu\text{m}/\text{h}$)
CL1-0 (2D, EF = 375) (from Ref. 9)	-0.005 ± 0.065	5.04 ± 0.74
CL1-0 (2DG, EF = 340)	0.04 ± 0.10	0.67 ± 0.05
CL1-0 (3D, EF = 338)	0.06 ± 0.05	3.63 ± 0.27
CL1-5 (2D, EF = 375) (from Ref. 9)	-0.60 ± 0.04	14.11 ± 0.86
CL1-5 (2DG, EF = 340)	-0.43 ± 0.08	11.55 ± 1.08
CL1-5 (3D, EF = 338)	-0.33 ± 0.10	11.56 ± 1.11
A549 (2D, EF = 300) (from Ref. 10)	0.76 ± 0.12	13.00 ± 2.50
A549 (2DG, EF = 340)	0.31 ± 0.10	3.88 ± 0.41
A549 (3D, EF = 375)	0.25 ± 0.04	7.73 ± 0.36

substrates (stiffness \sim GPa), and this difference in stiffness might affect cell attachment and subsequent electrotaxis and motility.^{83–85} From the current result, stiffer substrates result in more prominent electrotactic response of the cells. However, the effect of the steric hindrance cannot be ruled out. We plan to tune the stiffness of the scaffold to study the effect of stiffness on cell migration in 3D scaffold. The migration speed is also different in three environments, being 2D gelatin-coated glasses < 3D scaffolds < 2D bare substrates. Cells inside 3D scaffolds migrated slower than those on 2D bare substrates. There are two possible reasons for this result. The first one is again steric hindrance, which means cells inside scaffolds might be blocked by the walls. The second one is that cells inside scaffolds moved 3-dimensionally, while our observation was only 2-dimensional. The ignored *z*-dimension might reduce the actual migration speed of cells. The unexpected result of cells on 2D gelatin-coated glasses moving the slowest remained to be further investigated. Moreover, by comparing Fig. 6 (ellipticity) with Table III (speed), for 2DG vs. 3D of A549 cells, the abrupt decrease in ellipticity results in significant increase in migration speed. Similar speed increase was not observed for CL1-5. This indicates that the motility in EF is not solely determined by the steric hindrance caused by the cell shape.

IV. CONCLUSION

Here, we reported a study of electrotaxis of lung cancer cells in the alveoli-like 3D scaffolds and found that cells responded differently from those cultured on traditional 2D substrates. Inside such scaffolds, cells were able to migrate through interconnected pores to the neighboring big pore in response to electrical stimuli. With a similarity to what were observed in 2D environments, inside such 3D scaffolds, CL1-0 cells showed no clear electrotactic response, while CL1-5 cells moved toward the anode and A549 cells migrated toward the cathode. Under EF stimuli, cells respond differently in 2D and 3D environments, mainly due to the difference in materials, stiffness, spatial freedom, and steric hindrance. Especially, the finding that the directedness is proportional to the stiffness of cells' resting environment encourages us to keep on studying such dependence in 3D surroundings. Also, CL1-5 and A549 cells preferred round-shaped morphology when cultured in 3D scaffolds, in contrast to those having ellipse-shaped morphology in 2D substrates. This phenomenon can be again attributed to the stiffness of materials and the microstructure, in which cells were attached to and can also be related to the above-mentioned electrostatic responses. Our experimental results further suggest that it is of great importance to study cells' behaviors and functions in such 3D scaffolds mimicking the *in vivo* environments inside a human body.

ACKNOWLEDGMENTS

The financial support from National Science Council Taiwan (NSC Taiwan Contract No. NSC-98-2113 -M-001-013-MY2 and NSC-100-2113 -M-001-014-MY3) is acknowledged.

- ¹E. H. Du Bois-Reymond, *Untersuchungen Über Thierische Elektrizität* (G. Reimer, Berlin, 1848).
- ²C. D. McCaig, A. M. Rajnicek, B. Song, and M. Zhao, *Physiol. Rev.* **85**(3), 943 (2005).
- ³G. Tai, B. Reid, L. Cao, and M. Zhao, *Methods Mol. Biol.* **571**, 77 (2009).
- ⁴R. B. Borgens, A. R. Blight, D. J. Murphy, and L. Stewart, *J. Comp. Neurol.* **250**(2), 168 (1986).
- ⁵M. Levin, *Semin. Cell Dev. Biol.* **20**(5), 543 (2009).
- ⁶R. Nuccitelli, *Radiat. Prot. Dosim.* **106**(4), 375 (2003).
- ⁷F. Lin, F. Baldessari, C. C. Gyenge, T. Sato, R. D. Chambers, J. G. Santiago, and E. C. Butcher, *J. Immunol.* **181**(4), 2465 (2008).
- ⁸J. Li, S. Nandagopal, D. Wu, S. F. Romanuik, K. Paul, D. J. Thomson, and F. Lin, *Lab Chip* **11**(7), 1298 (2011).
- ⁹C. W. Huang, J. Y. Cheng, M. H. Yen, and T. H. Young, *Biosens. Bioelectron.* **24**(12), 3510 (2009).
- ¹⁰X. L. Yan, J. Han, Z. P. Zhang, J. Wang, Q. S. Cheng, K. X. Gao, Y. F. Ni, and Y. J. Wang, *Bioelectromagnetics (N.Y.)* **30**(1), 29 (2009).
- ¹¹J. Zhang, M. Calafiore, Q. Zeng, X. Zhang, Y. Huang, R. A. Li, W. Deng, and M. Zhao, *Stem Cell Rev.* **7**(4), 987 (2011).
- ¹²B. Rapp, A. Deboisfleurychevance, and H. Gruler, *Eur. Biophys. J.* **16**(5), 313 (1988).
- ¹³P. C. T. Chang, G. L. Sulik, H. K. Soong, and W. C. Parkinson, *J. Formos Med. Assoc.* **95**(8), 623 (1996).
- ¹⁴M. Zhao, H. Bai, E. Wang, J. V. Forrester, and C. D. McCaig, *J. Cell Sci.* **117**(3), 397 (2004).
- ¹⁵M. S. Cooper and R. E. Keller, *Proc. Natl. Acad. Sci. U.S.A.* **81**(1), 160 (1984).

- ¹⁶D. M. Sheridan, R. R. Isseroff, and R. Nuccitelli, *J. Invest. Dermatol.* **106**(4), 642 (1996).
- ¹⁷E. K. Onuma and S. W. Hui, *Cell Calcium* **6**(3), 281 (1985).
- ¹⁸M. B. A. Djamgoz, M. Mycielska, Z. Madeja, S. P. Fraser, and W. Korohoda, *J. Cell Sci.* **114**(Pt 14), 2697 (2001).
- ¹⁹J. Pu, C. D. McCaig, L. Cao, Z. Zhao, J. E. Segall, and M. Zhao, *J. Cell Sci.* **120**(Pt 19), 3395 (2007).
- ²⁰B. Song, Y. Gu, J. Pu, B. Reid, Z. Q. Zhao, and M. Zhao, *Nat. Protoc.* **2**(6), 1479 (2007).
- ²¹F. Boukhechba, T. Balaguer, J. F. Michiels, K. Ackermann, D. Quincey, J. M. Boulter, W. Pyerin, G. F. Carle, and N. Rochet, *J. Bone Miner. Res.* **24**(11), 1927 (2009).
- ²²I. Kim, H. Park, Y. Shin, and M. Kim, *J. Tissue Eng. Regener. Med.* **6**(4–11), 924 (2009).
- ²³H. Liu and K. Roy, *Tissue Eng.* **11**(1–2), 319 (2005).
- ²⁴T. Ma, Y. Li, S. T. Yang, and D. A. Kniss, *Biotechnol. Bioeng.* **70**(6), 606 (2000).
- ²⁵X. F. Tian, B. C. Heng, Z. Ge, K. Lu, A. J. Rufaihah, V. T. W. Fan, J. F. Yeo, and T. Cao, *Scand. J. Clin. Lab. Invest.* **68**(1), 58 (2008).
- ²⁶T. Nakamura, Y. Kato, H. Fujii, T. Horiuchi, Y. Chiba, and K. Tanaka, *Int. J. Mol. Med.* **12**(5), 693 (2003).
- ²⁷J. Yin, Q. Meng, G. L. Zhang, and Y. H. Sun, *Chem. Biol. Interact.* **180**(3), 368 (2009).
- ²⁸D. Loessner, K. S. Stok, M. P. Lutolf, D. W. Hutmacher, J. A. Clements, and S. C. Rizzi, *Biomaterials* **31**(32), 8494 (2010).
- ²⁹Q. Meng, *Expert Opin. Drug Metab. Toxicol.* **6**(6), 733 (2010).
- ³⁰J. L. Horning, S. K. Sahoo, S. Vijayaraghavalu, S. Dimitrijevic, J. K. Vasir, T. K. Jain, A. K. Panda, and V. Labhassetwar, *Mol. Pharmacol.* **5**(5), 849 (2008).
- ³¹T. K. Kim, B. Sharma, C. G. Williams, M. A. Ruffner, A. Malik, E. G. McFarland, and J. H. Elisseeff, *Osteoarthritis Cartilage* **11**(9), 653 (2003).
- ³²G. N. Li, L. L. Livi, C. M. Gourde, E. S. Deweerd, and D. Hoffman-Kim, *Tissue Eng.* **13**(5), 1035 (2007).
- ³³S. Li, J. Lao, B. P. Chen, Y. S. Li, Y. Zhao, J. Chu, K. D. Chen, T. C. Tsou, K. Peck, and S. Chien, *FASEB J.* **17**(1), 97 (2003).
- ³⁴S. R. Peyton, C. B. Raub, V. P. Keschrumrus, and A. J. Putnam, *Biomaterials* **27**(28), 4881 (2006).
- ³⁵Y. B. Xie, S. T. Yang, and D. A. Kniss, *Tissue Eng.* **7**(5), 585 (2001).
- ³⁶M. Bokhari, R. J. Carnachan, N. R. Cameron, and S. A. Przyborski, *J. Anat.* **211**(4), 567 (2007).
- ³⁷H. J. Boxberger and T. F. Meyer, *Biol. Cell* **82**(2–3), 109 (1994).
- ³⁸Z. Z. Wu, Y. P. Zhao, and W. S. Kisaalita, *Biosens. Bioelectron.* **22**(5), 685 (2006).
- ³⁹T. Tsunoda, B. Furusato, Y. Takashima, S. Ravulapalli, A. Dobi, S. Srivastava, D. G. McLeod, I. A. Sesterhenn, D. K. Ornstein, and S. Shirasawa, *Prostate* **69**(13), 1398 (2009).
- ⁴⁰S. I. Fraley, Y. F. Feng, R. Krishnamurthy, D. H. Kim, A. Celedon, G. D. Longmore, and D. Wirtz, *Nat. Cell Biol.* **12**(6), 598 (2010).
- ⁴¹H. Peretz, A. E. Talpalar, R. Vago, and D. Baranes, *Tissue Eng.* **13**(3), 461 (2007).
- ⁴²S. Scaglione, A. Braccini, D. Wendt, C. Jaquierey, F. Beltrame, R. Quarto, and I. Martin, *Biotechnol. Bioeng.* **93**(1), 181 (2006).
- ⁴³R. M. Quiros, M. Valianou, Y. Kwon, K. M. Brown, A. K. Godwin, and E. Cukierman, *Gynecol. Oncol.* **110**(1), 99 (2008).
- ⁴⁴B. C. Mehta, D. W. Holman, D. M. Grzybowski, and J. J. Chalmers, *Tissue Eng.* **13**(6), 1269 (2007).
- ⁴⁵C. C. Ceresa, A. J. Knox, and S. R. Johnson, *Am. J. Physiol. Lung Cell. Mol. Physiol.* **296**(6), L1059 (2009).
- ⁴⁶T. Luhmann, P. Hanseler, B. Grant, and H. Hall, *Biomaterials* **30**(27), 4503 (2009).
- ⁴⁷I. Grabowska, A. Szeliga, J. Moraczewski, I. Czaplicka, and E. Brzoska, *Cell Biol. Int.* **35**(2), 125 (2010).
- ⁴⁸C. Chen, K. Chen, and S. T. Yang, *Biotechnol. Prog.* **19**(5), 1574 (2003).
- ⁴⁹V. Chopra, T. V. Dinh, and E. V. Hannigan, *in vitro Cell. Dev. Biol.: Anim.* **33**(6), 432 (1997).
- ⁵⁰T. Okamoto, M. Takagi, T. Soma, H. Ogawa, M. Kawakami, M. Mukubo, K. Kubo, R. Sato, K. Toma, and T. Yoshida, *Int. J. Artif. Organs* **7**(4), 194 (2004).
- ⁵¹Y. Torisawa, H. Shiku, T. Yasukawa, M. Nishizawa, and T. Matsue, *Biomaterials* **26**(14), 2165 (2005).
- ⁵²A. Desai, W. S. Kisaalita, C. Keith, and Z. Z. Wu, *Biosens. Bioelectron.* **21**(8), 1483 (2006).
- ⁵³J. R. Merwin, J. M. Anderson, O. Kocher, C. M. Van Itallie, and J. A. Madri, *J. Cell Physiol.* **142**(1), 117 (1990).
- ⁵⁴K. Storch, I. Eke, K. Borgmann, M. Krause, C. Richter, K. Becker, E. Schrock, and N. Cordes, *Cancer Res.* **70**(10), 3925 (2010).
- ⁵⁵C. S. Ki, S. Y. Park, H. J. Kim, H. M. Jung, K. M. Woo, J. W. Lee, and Y. H. Park, *Biotechnol. Lett.* **30**(3), 405 (2008).
- ⁵⁶C. L. Li, T. Tian, K. J. Nan, N. Zhao, Y. H. Guo, J. Cui, J. Wang, and W. G. Zhang, *Oncol. Rep.* **20**(6), 1465 (2008).
- ⁵⁷J. Luo and S. T. Yang, *Biotechnol. Prog.* **20**(1), 306 (2004).
- ⁵⁸R. B. Dickinson and R. T. Tranquillo, *AIChE J.* **39**(12), 1995 (1993).
- ⁵⁹M. Ehrbar, A. Sala, P. Lienemann, A. Ranga, K. Mosiewicz, A. Bittermann, S. C. Rizzi, F. E. Weber, and M. P. Lutolf, *Biophys. J.* **100**(2), 284 (2011).
- ⁶⁰L. A. Ma, C. C. Zhou, B. Y. Lin, and W. Li, *Biomed. Microdevices* **12**(4), 753 (2010).
- ⁶¹B. B. Mandal and S. C. Kundu, *Biomaterials* **30**(15), 2956 (2009).
- ⁶²C. F. Tu, Q. Cai, J. Yang, Y. Q. Wan, J. Z. Bei, and S. Wang, *Polym. Adv. Technol.* **14**(8), 565 (2003).
- ⁶³Y. X. Huang, J. Ren, C. Chen, T. B. Ren and X. Y. Zhou, *J. Biomater. Appl.* **22**(5), 409 (2008).
- ⁶⁴A. K. Ekaputra, G. D. Prestwich, S. M. Cool, and D. W. Hutmacher, *Biomacromolecules* **9**(8), 2097 (2008).
- ⁶⁵D. M. Xie, H. M. Huang, K. Blackwood, and S. MacNeil, *Biomed Mater* **5**, 065016 (2010).
- ⁶⁶M. Y. Li, Y. Guo, Y. Wei, A. G. MacDiarmid, and P. I. Lelkes, *Biomaterials* **27**(13), 2705 (2006).
- ⁶⁷Y. H. Gong, Z. W. Ma, Q. L. Zhou, J. Li, C. Y. Gao, and J. C. Shen, *J. Biomater. Sci., Polym. Ed.* **19**(2), 207 (2008).
- ⁶⁸J. G. Fernandez and A. Khademhosseini, *Adv Mater* **22**(23), 2538 (2010).
- ⁶⁹I. Zein, D. W. Hutmacher, K. C. Tan, and S. H. Teoh, *Biomaterials* **23**(4), 1169 (2002).
- ⁷⁰K. G. Marra, J. W. Szem, P. N. Kumta, P. A. DiMilla, and L. E. Weiss, *J. Biomed. Mater. Res.* **47**(3), 324 (1999).
- ⁷¹W. L. Wang, C. M. Cheah, J. Y. H. Fuh, and L. Lu, *Mater. Des.* **17**(4), 205 (1996).
- ⁷²J. T. Rimell and P. M. Marquis, *J. Biomed. Mater. Res.* **53**(4), 414 (2000).
- ⁷³R. A. Giordano, B. M. Wu, S. W. Borland, L. G. Cima, E. M. Sachs, and M. J. Cima, *J. Biomat. Sci., Polym. Ed.* **8**(1), 63 (1996).

- ⁷⁴K. Y. Chung, N. C. Mishra, C. C. Wang, F. H. Lin, and K. H. Lin, *Biomicrofluidics* **3**, 022403 (2009).
- ⁷⁵J.-Y. Lin, W.-J. Lin, W.-H. Hong, H.-H. Ning, W.-C. Hung, S. H. Nowotarski, S. M. Gouveia, I. Cristo, and K.-H. Lin, *Soft Matter* **7**, 10010 (2011).
- ⁷⁶X. F. Li and J. Kolega, *J. Vasc. Res.* **39**(5), 391 (2002).
- ⁷⁷J. Y. Shih, S. C. Yang, T. M. Hong, A. Yuan, J. J. W. Chen, C. J. Yu, Y. L. Chang, Y. C. Lee, K. Peck, C. W. Wu, and P. C. Yang, *J. Natl. Cancer Inst.* **93**(18), 1392 (2001).
- ⁷⁸J. J. W. Chen, K. Peck, T. M. Hong, S. C. Yang, Y. P. Sher, J. Y. Shih, R. Wu, J. L. Cheng, S. R. Roffler, C. W. Wu, and P. C. Yang, *Cancer Res.* **61**(13), 5223 (2001).
- ⁷⁹Y. W. Chu, P. C. Yang, S. C. Yang, Y. C. Shyu, M. J. C. Hendrix, R. Wu, and C. W. Wu, *Am. J. Respir. Cell Mol. Biol.* **17**(3), 353 (1997).
- ⁸⁰M. R. Buckley, J. P. Gleghorn, L. J. Bonassar, and I. Cohen, *J. Biomech.* **41**, 2430 (2008).
- ⁸¹J. D. Mih, D. J. Tschumperlin, *Proc. Am. Thorac. Soc.* **5**, 2 (2008).
- ⁸²C.-W. Huang, H.-Y. Chen, M.-H. Yen, J. J. W. Chen, T.-H. Young, and J.-Y. Cheng, *PLoS ONE* **6**(10), e25928 (2011).
- ⁸³D. E. Discher, P. Janmey, and Y. L. Wang, *Science* **310**(5751), 1139 (2005).
- ⁸⁴S. R. Peyton, Z. I. Kalcioğlu, J. C. Cohen, A. P. Runkle, K. J. Van Vliet, D. A. Lauffenburger, and L. G. Griffith, *Biotechnol. Bioeng.* **108**(5), 1181 (2011).
- ⁸⁵T. Yeung, P. C. Georges, L. A. Flanagan, B. Marg, M. Ortiz, M. Funaki, N. Zahir, W. Y. Ming, V. Weaver, and P. A. Janmey, *Cell Motil. Cytoskeleton* **60**(1), 24 (2005).

Biomicrofluidics is published by the American Institute of Physics. Copyright (c) 2006 American Institute of Physics. All rights reserved. No claim is made to original U.S. Government works.